Nanoscale Advances

REVIEW

View Article Online
View Journal | View Issue

Cite this: *Nanoscale Adv.*, 2026, **8**, 794

Synthetic methodologies of gold nanorod@MOF nanohybrids focused on biological applications

Catherine E. Araneda, [ab] Aldo A. Campos, [b] Monica Soler [*b] and Marcelo J. Kogan [*ac]

A stable and controllable coating can be formed on the surface of gold nanorods (AuNRs) by using metal–organic frameworks (MOFs), which avoids the agglomeration of the nanohybrid AuNR@MOF and also expands the functionality of the plasmon nanoparticles. In this review, we discuss the chemical role of the different components of the nanohybrid, *i.e.*, AuNR, surface ligand or mesoporous nanostructure (MN) and the MOF around the AuNR. The methodologies used in the different synthesis stages and the factors to be considered to maintain stability in the construction of this type of nanostructures are also reported. Furthermore, we observed that there are a wide variety of MOF morphologies that can be built around AuNRs, even using the same components for their formation, which vary depending on the synthesis methodology. Finally, we discuss about the broad range of applications, of the AuNR@MOF nanohybrids, mainly in the biological field.

Received 28th August 2025
Accepted 2nd December 2025

DOI: 10.1039/d5na00832h

rsc.li/nanoscale-advances

1. Introduction

Many researchers have successfully developed different synthetic methodologies to prepare gold nanoparticles (AuNPs) with controllable sizes and shapes, such as stars, spheres, prisms, and rods,[1,2] looking to control their optical properties. Among the different shapes studied, gold nanorods (AuNRs) have been intensively and particularly studied owing to their optical properties ranging from visible to near-infrared (NIR) region by adjusting the aspect ratio.[3,4] NIR is also called the biological window, which is especially relevant to biological systems due to the high penetration of the irradiation into the tissues. This attribute makes AuNRs good candidates for nanomedicine applications.[5]

AuNPs have the capacity to cause a phenomenon known as localized surface plasmon resonance (LSPR), which implies that when AuNPs are excited with light, the applied electromagnetic field interacts with their surfaces and the outermost electrons begin to vibrate, generating a kind of vibrating electronic cloud known as plasmon. Once AuNPs are excited with light, they can emit the energy received through light scattering, resulting in a phenomenon known as surface-enhanced fluorescence (SEF). This phenomenon can be used in nanosystems containing AuNRs and a chromophore where the incident light excites both species, but the scattering light generated by the plasmon also manages to excite the chromophore, as long as the distance between the surface of AuNRs and the chromophore is adequate, increasing the intensity of its fluorescence emission. To date, this distance has been reported to be generated with a peptide[6] or a core–shell of SiO_2,[7] for example. AuNPs can also generate the surface-enhanced Raman scattering (SERS) effect, which is used for high-sensitivity analyte detection.[8–10] This effect produces an intense dramatic enhancement in the detection of the analyte located adjacent to metal nanostructures. In particular, AuNRs have emerged as a powerful analytical technique for monitoring trace amounts of chemical and biological analytes because of their longitudinal plasmon band. AuNRs can be easily tuned by changing the aspect ratio to match the excitation laser for the maximum Raman enhancement, high sensitivity, and rapid response,[11,12] for instance. Finally, hybrid nanostructures based on AuNRs encapsulated within MOFs, abbreviated as AuNR@MOF, have been reported, where they can take up molecules into the MOF pores, bringing them close to the AuNR surface, which has the advantage of facilitating highly selective detection, allowing efficient detection of guest molecules by SERS.[13,14]

MOFs are structures formed by the assembly of metal ions or even preformed clusters of metal ions, which act as metal centers connected to one or more kinds of organic linkers, forming 1D, 2D or 3D porous coordination polymers.[15,16] These crystalline structures are micro-/nanoscale in size, have a large surface area, and contain nanopores with controllable pore size and geometry depending on the synthesis conditions appropriate for the required design, allowing MOFs to be used in various applications, including gas storage and separation,

[a]*Department of Pharmacological and Toxicological Chemistry, Faculty of Chemical and Pharmaceutical Sciences, University of Chile, Santos Dumont 964, Santiago, Chile. E-mail: mkogan@ciq.uchile.cl*

[b]*Department of Chemical Engineering, Biotechnology and Materials, Faculty of Physical Sciences and Mathematics, University of Chile, Beauchef 851, Santiago, Chile. E-mail: msoler@ing.uchile.cl*

[c]*Advanced Center of Chronic Diseases (ACCDiS), Chile*

environmental gas sensing, catalysis of chemical reactions, transport of drugs or molecules and metal ions, and fluorescence sensing.[17–22]

Recently, AuNP@MOF hybrid nanostructures have been reported in the literature and used in several applications, including sensing,[23–27] catalysis[28–30] and analyte detection.[31,32] The preparation of these nanostructures can present certain new advantages as follows: (i) MOFs can be used to prevent AuNP agglomeration;[33] (ii) MOFs can form a protective shell around the AuNP with a controllable size; and (iii) as hybrid materials, they can improve their properties, eliciting a selective and higher catalytic activity and improving selectivity for small analytes, and significant improvement of sensitivity for Raman detection is possible as well, which is hardly achieved by either AuNPs or MOFs alone.[31,34] These advantages are the principal reason for the preparation of such new hybrid materials.

Some research groups have studied particularly AuNR@MOF nanohybrids[13,14,35–46] and help us understand the role of their components, the synthesis methodologies involved and the applications for which they can be used based on the characteristics of AuNRs and MOFs. Indeed, these nanohybrids are especially interesting because of their distinct optical properties. In addition, these materials have demonstrated several applications, including protein sponge[35] and imaging-guided tumor diagnosis,[42] killing or damaging cancer cells,[37,40,44] drug loading efficiency, NIR light-triggered drug release and biological imaging, controlled molecule release,[38] molecular capture or blockage[41] and SERS effect.[13,14] Moreover, there are other AuNR@MOF nanohybrids that have potential applications in areas such as catalysis,[36] photocatalysis and nanomedicine[39,45] and synthesis of new MOFs around AuNRs.[43,46]

In general, the synthetic methods to encapsulate NPs by MOFs can be classified into three strategies: (A) preformed NPs are then coated with a MOF around (Fig. 1A), (B) NPs are grown inside a preformed MOF (Fig. 1B and C) NPs and MOF are grown at the same time, where NPs generally remain embedded within the MOF (Fig. 1C).[47] Besides, the number of NPs embedded within a MOF is relative and will basically depend on the properties of the precursors and the synthesis methodology in general.

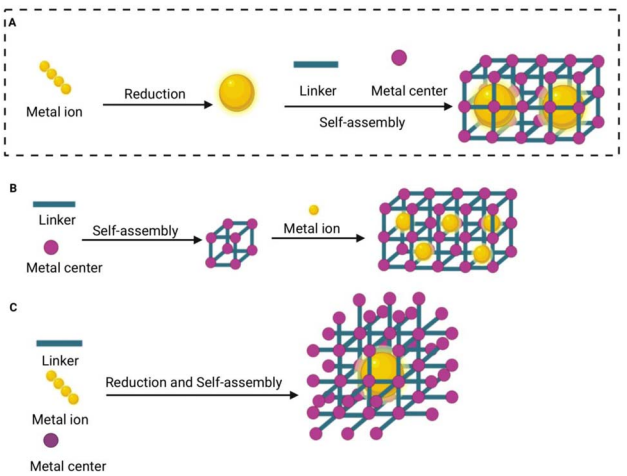

Fig. 1 Schematic of the strategies for obtaining NPs surrounded by MOFs. (A) NPs which are subsequently covered with a MOF shell. (B) NPs growing inside a preformed MOF. (C) NPs and MOF growing at the same time.

For the preparation of AuNR@MOF nanohybrids, AuNRs must be functionalized with a surface ligand, by a self-assembled monolayer (SAM), or surrounded by the combination of a mesoporous nanostructure shell, also known as MN shell, and a SAM, before initiating the MOF synthesis, facilitating, and allowing the initiation of its growth. As mentioned before, MOF structures are synthesized by the combination of linkers and either metal ions or preformed clusters. It is said that, to help the formation of the MOF around the AuNRs, it is convenient to generate the MOF using clusters, since the cluster is preformed, introducing less steps in the MOF growth. However, the linker can also be added in the form of a salt, which could allow a faster interaction with the metal center to be used and avoid agglomeration, controlling the reaction medium charge, thus stabilizing MOF growth synthesis.[36]

Based on the above, we present an exhaustive analysis of the role of the training components and the different methodologies such as layer-by-layer (LbL), microwave, solvothermal or stirring techniques used to synthesize AuNR@MOF hybrid nanostructures following the general strategy A, considering that the synthesis of the AuNR with a rod-like morphology occurs before coating it with the MOF. In addition, we summarize their applications, which have been used mainly in biology due to the complementary properties of AuNRs and MOFs.

2 Synthesis of AuNRs

The synthesis of AuNRs has been reported to involve seed-mediated growth. The seeds are obtained from an aqueous solution of chloroauric acid ($HAuCl_4$) in the presence of a strong reducer such as sodium borohydride ($NaBH_4$), capable of reducing Au^{3+} to Au^0.[48] In addition, the presence of a cationic surfactant such as hexadecyltrimethylammonium bromide (CTAB) is important because it helps to stabilize the seeds preventing aggregation once they are formed in the solution. Once the precursor seed solution is obtained, a part of this is added to the growth solution. This solution contains: (i) $HAuCl_4$ that induces seed growth, (ii) a weak reductant, which is normally ascorbic acid ($C_6H_8O_6$), (iii) a silver salt such as silver nitrate ($AgNO_3$) and (iv) the seed solution previously prepared. In the presence of CTAB, $C_6H_8O_6$ present in the growth solution reduces Au^{3+} to Au^{1+}. When the Au^0 seed solution is added to the growth solution containing Au^{1+}, this last one can be reduced due to the transfer of electrons from the surface of the Au^0 seeds.[49]

2.1 Growth mechanism of AuNRs

This plasmonic nanoparticle consists of a 3D morphology based on a pentagonally twinned prism, where each end of the rod is capped with five triangular faces that are Au {111}. The sides of the rods are not as well-defined; either the Au {100} or the Au

{110} face, or both (Fig. 2A). Another important factor to highlight is that the growth occurs in the [110] direction (Fig. 2B).

It is proposed that the formation mechanism of rods proposed induces preferential binding of the CTAB trimethylammonium head groups to the {100} faces of Au existing along the sides of rods, as compared to the {111} faces at the tips. In the growth process, CTAB coats the AuNR in a bilayer fashion with the head groups of the first and second monolayer facing and opposite to the Au {100} faces mainly, respectively.[50] Besides, the presence of $AgNO_3$ in the growth solution helps to control the AuNR morphology by increasing its proportion, that is, it improves the performance in percentage of the AuNRs.[3] One of the explanations for the role of silver salt in controlling the plasmon morphology is based on the preferential growth of some directions over others. When silver ions are present, they combine bromide ions from CTAB to generate AgBr, which binds to the growth surfaces of the AuNRs, catalyzing the elongation process in the [110] direction of the plasmon and increasing the aspect ratio.[51] It is important to mention that the seed-mediated silver-assisted AuNR synthesis is the most well-developed, scalable, and tunable method to date. In addition, there are undoubtedly other species on the AuNR surface that are formed during the synthesis, which have been described by Murphy and collaborators in detail.[52]

The articles related to the formation of AuNR@MOF[13,14,35–46] nanohybrids do not necessarily use the same weak reducer for the AuNR synthesis, and $C_6H_8O_6$[13,14,37–42,44–46] and hydroquinone ($C_6H_6O_2$)[35,36] are the ones that have been used. Moreover, a strong reducer ($NaBH_4$), surfactant (CTAB) and silver nitrate ($AgNO_3$) can be found in different concentrations according to these research works (Table 1), which influences the size of AuNRs.

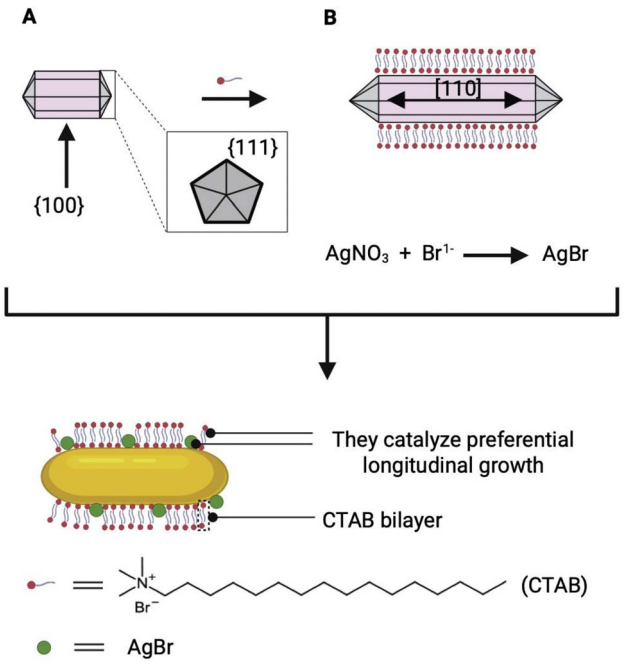

Fig. 2 Representation of (A) Au faces and (B) the influence of CTAB and AgBr on the growth of AuNRs in the [110] direction.

Table 1 Summary of $AgNO_3$ concentration and AuNR size generated in the synthesis

$AgNO_3$ [mM]	AuNR size (length × width nm)	Ref.
10	86 ± 16 × 23 ± 3	36
10	67 ± 9 × 18 ± 4	35
4	—[b]	42
4	47 × 12	44
4	∼ 56 × ∼ 13	37
—[b]	—[b]	39
4	—[b]	38
4	—[b]	41
10	—[b]	13
—[b]	44 ± 8 × 10 ± 1	14
4	—[b]	40
0.06	∼ 40 × 10	45
10	—[b]	46[a]

[a] In the preparation of Au seed, not only $HAuCl_4$ and $NaBH_4$ are used but also trisodium citrate ($Na_3C_6H_5O_7$) which acts as a capping agent and thus restricts particle growth. For the preparation of growth solution, $HAuCl_4$ and CTAB are used, but acetone and cyclohexane are also added. The role of acetone is to loosen the micellar framework, and cyclohexane is necessary for enhancing the rod-like micellar structure. Another interesting factor is that CTAB was added as a solid in the preparation of the two solutions, *i.e.*, seed and growth solution. The details of synthesis are explained in the work carried out by Jana *et al.*[53] [b] Not reported.

Based on the above, the synthesis of AuNRs has the advantage of being able to modify the rod size using the same starting reagents. However, it has disadvantages as well, as it is generally sensitive to changes in reactant concentration, temperature, reaction times, and inadequate stirring speeds.[3] This can affect optimal production, possibly leading to agglomeration and/or decomposition.

2.2 Characterization techniques

Through the UV-vis absorbance spectroscopy, it is possible to observe that AuNRs absorb in two wavelength ranges, around ∼500 nm and ∼1200 nm,35 corresponding to the transversal and longitudinal plasmon bands, respectively (Fig. 3A). However, their values will depend on their chemical environment that can be affected by a surfactant, organic ligand or a MOF on the plasmon surface, shifting (towards the near- or far-infrared region), intensifying and/or broadening the plasmon absorbance.[3,36] After excitation, AuNRs disperse energy and/or emit it in the form of heat. Using powder X-ray diffraction (PXRD), it is possible to confirm the formation of AuNRs through their characteristic diffraction planes. In the diffraction pattern of AuNR@MOF nanohybrids, more and new planes can be observed due to the chemical environment generated by MOFs around the plasmon (Fig. 3B). Another characterization technique used for AuNR@MOF nanohybrids is the ζ-potential, which allows us to know the superficial charge, which depends on the surfactant or surface ligand around the Au, to give an example (Fig. 3C). Transmission electron microscopy (TEM) (Fig. 3D) and scanning electron microscopy (SEM) techniques can give us a value of the transversal and longitudinal sizes of AuNRs,[54] in addition to allowing us to observe their

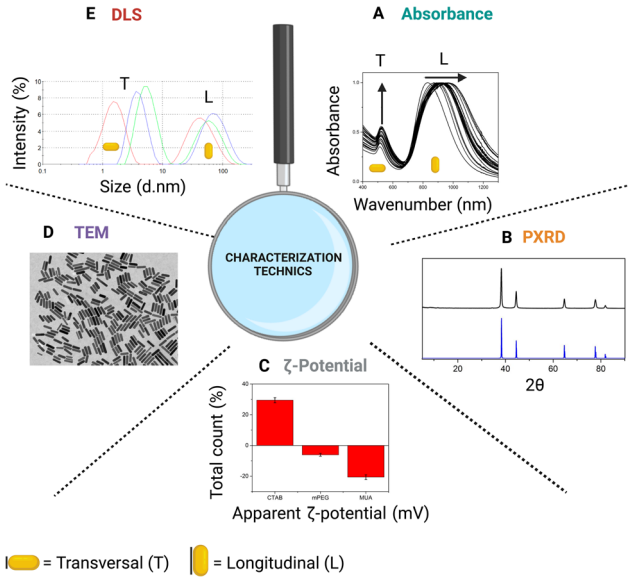

Fig. 3 AuNR characterization techniques that together allow us to unambiguously confirm its formation and the effects of chemical environment that modify the characterizations. (A) UV-vis spectra of the AuNRs with MOF shells generated by LbL methodology. As layers are added, the transversal plasmon intensity increases, while the longitudinal plasmon shifts into the NIR region and broadness, as indicated by the arrows. (B) PXRD patterns of MOF-coated AuNRs (black) along with a AuNR (blue). (C) ζ-potential of AuNR solutions with various surface ligands, such as CTAB, (polyethylene glycol) PEG and 11-mercaptoundecanoic acid (MUA), which vary the value of the surface charge around Au. (D) TEM images of AuNRs. Reproduced from ref. 36. Copyright 2018 ACS Publications. (E) DLS graphic of AuNR-CTAB (red line), AuNR-PEG (green line) and AuNR-PEG-D1 (D1 acts as the biorecognition peptide) (blue line). Reproduced from ref. 3. Copyright 2020 MDPI.

morphology. Dynamic light scattering (DLS) technique allows us to have these sizes too (Fig. 3E) but with less precision than TEM or SEM.

3. Type of surface ligand or MN shell used to synthesize AuNR@MOF nanohybrids

To obtain AuNR@MOF nanohybrids, it is necessary to cover the AuNRs with surface ligands by SAM. The ligands used in the construction of these nanostructures have terminal functional groups adequate, on the one hand, to interact with the Au or Au-MN shell, and on the other hand, to initiate the MOF growth around the Au. The variety of surface ligands, their features (molecular weight (M_w), structure, functional groups, *etc.*), and reaction conditions that allow them to generate this dual function are presented below.

3.1 HS-PEG

Osterrieth *et al.*[41] replaced the CTAB capping ligand by HS-PEG (with $M_w = 2000$ g mol^{-1} and unspecified exposed termination) (Fig. 4A) using a phase-transfer method.[55] It is a simple and highly efficient protocol to transfer AuNRs from water to dichloromethane (DCM) organic solvent that contains HS-PEG upon the addition of methanol (MeOH). The addition of MeOH solvent that is miscible in both water and DCM is necessary for efficient and spontaneous transfer. Owing to the affinity of the thiol group for Au, the CTAB bilayer adsorbed onto the Au surface after the synthesis was displaced by the HS-PEG. The Au–S bond generated is covalent, since both elements are soft (Pearson's Theory), that is why Au and ligands are attracted to each other.[56] PEG was expected to interact with the Zr-based NU-901 MOF precursors due to its hard oxygen and soft ethylene moieties.

3.2 HS-$(CH_2)_2$ CO-NH-PEG-OH

Khaletskaya *et al.*[38] proposed a SAM with the HS-$(CH_2)_2$-CO-NH-PEG-OH ligand ($M_w = 3317$ g mol^{-1}) (Fig. 4B). Here AuNRs were purified by centrifugation to remove excess CTAB and were redispersed in water. The ligand was also dissolved in water, sonicated, and mixed with a $NaBH_4$ reducing agent (possibly to avoid Au oxidation). The mixture was sonicated again to prevent ligand dimerization (PEG-S-S-PEG). The solutions of AuNRs and PEG were mixed under vigorous stirring and sonicated. Excess PEG molecules were removed by repeated centrifugation.

Besides, AuNRs functionalized on the surface with PEG exhibited high stability and remained unaggregated. It is postulated that PEG assembled with AuNR interacts through hydrogen bonds with a subsequent attachment of amorphous

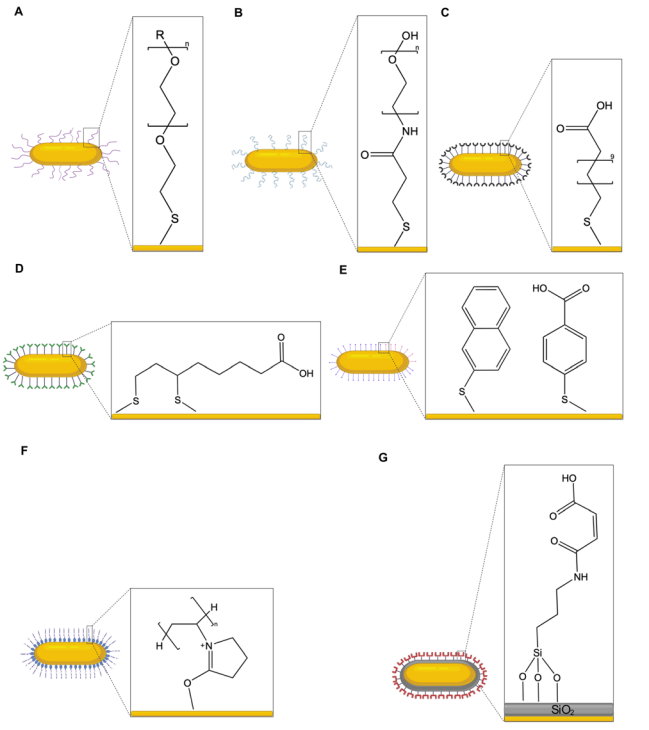

Fig. 4 Self-assembly with various surface ligands on AuNRs to facilitate the MOF shell growth. The ligands or MN used to be functionalized with AuNRs to date are: (A) HS-PEG; (B) HS-$(CH_2)_2$ CO-NH-PEG-OH; (C) MUA; (D) LA; (E) NPT (left) and MBA (right); (F) PVP; and (G) MSN-COOH.

alumina to the plasmon surface. Then there was a linker addition that has the objective of finishing generating the $[Al(OH)(1,4ndc)]_n$ structure around AuNRs, as will be explained in detail later.

3.3 11-Mercaptoundecanoic acid (MUA)

(i) In a synthesis process used by Hinman *et al.*,[36] AuNR-CTAB was initially washed with nanopure water by centrifugation to remove CTAB, and then the first SAM with a HS-PEG (M_w = 5000 g mol^{-1}) was synthesized in nanopure water, with the goal of transferring the AuNRs into an organic solvent without causing particle aggregation. This ligand has a thiol group at one end capable of chemisorbing to the Au surface. Afterward, the excess of HS-PEG was removed by centrifugation with nanopure water, and then the AuNRs were also self-assembled with MUA (dissolved in the organic solvent ethanol (EtOH)) in nanopure water. PEG ligands have a bigger size and more inter- and intramolecular interactions than MUA, due to the less dense layer on the Au surface.[57] This leaves space for smaller thiolate MUA ligands to bind to the AuNRs and form SAMs that displace PEGs (which facilitates ligand exchange in the presence of EtOH avoiding aggregation) around Au. AuNRs that are already functionalized with small thiolate ligands are not as readily accessible for ligand exchange on the AuNR surface. In order to leave the exposed end of the MUA with a negative charge, *i.e.,* COO^-, a sodium hydroxide salt (NaOH) was added. This allows the AuNR-MUA (Fig. 4C) to interact more easily with the metal center to initiate in this case the Cu-based HKUST-1 (1) MOF growth in EtOH (organic solvent).

(ii) In the Shang *et al.*[42] strategy, CTAB ligands on the surface of the AuNRs were directly exchanged for MUA. Initially, the AuNRs were concentrated by centrifugation. Then, the supernatant was removed, and water was added to prepare an ultrasonic dispersion. Next, water and MUA (in an EtOH solution) were added to the Au dispersion without passing through a PEG ligand. The mixture was sonicated and incubated at room temperature (r.t.) with the AuNRs. The solution was centrifuged to collect the MUA-capped AuNRs. It not only gives rise to MUA assembled with AuNRs, which then is going to interact with the metal center and linker, respectively, to generate the Fe-based MIL-88 (A) MOF, but also eliminate the cytotoxicity of the surfactant.

(iii) In one of the works of Sugikawa *et al.*[13] the replacement of CTAB for MUA was carried out by adding MUA (in EtOH solution) to CTAB-capped AuNRs under ultrasonication at 30 °C and then the pH was adjusted to 11.3 with aqueous NaOH (generating COO^- at the exposed end of MUA to prevent aggregation). The obtained MUA-capped AuNRs showed a blue shift of the longitudinal surface plasmon band by absorbance, which is due to the change in local refractive index produced by MUA capping. After SAM, the Zn-based MOF (1) shell was synthesized around MUA-capped AuNRs.

(iv) In another work of Sugikawa *et al.*[14] the CTAB-capped AuNR solution was centrifuged, and the supernatant was disposed to remove the excess of CTAB. The CTAB-capped AuNRs was redispersed in water and centrifuged again. After removal of the supernatant, water and MUA (in EtOH solution) were added. The mixed solution was kept under constant sonication and then incubated at r.t. The solution was centrifuged to collect MUA-capped AuNRs to then use it to initiate the growth of MOF-5 also based on Zn as the metal center.

3.4 Lipoic acid (LA)

To synthesize the nanoparticle-induced heterogeneous nucleation, Zeng *et al.*[39,40] in two different studies functionalized AuNRs with LA using the same methodology. At first, the obtained AuNRs were centrifuged followed by washing with water to remove excess CTAB surfactants. After discarding the supernatant, the AuNRs were redispersed in water. LA in EtOH and a HS-PEG (with size and exposed termination unspecified) to avoid aggregation were added to the Au dispersion under gentle stirring and left to react at r.t. After that, excess of LA and HS-PEG ligands were removed by repeated centrifugation. The LA ligand has the particularity of having a S–S bridge contained in a pentacycle that is part of its structure, and in the reaction, a self-assembled monolayer of LA was formed on the Au surface with two Au–S covalent bonds (Fig. 4D).[58] After the functionalization, LA-capped AuNRs possess high physical-chemical stability, which can be used as the core for heterogeneous nucleation where the porphyrin MOFs, MOF (2)[39] and MOF (3),[40] grow (both based on Zr and porphyrin as linkers), due to the coordination interactions between the LA carboxyl groups around the AuNR and the MOF metal nodes.

3.5 2-Naphthalenethiol (NPT) and 4-mercaptobenzoic acid (MBA)

In this work, He *et al.*[43] reported a facile strategy that controls the growth of the ZIF-8 (1) MOF on the surface of AuNRs (purchased) in a colloidal solution at r.t. The selective growth was driven by surface functionalization of AuNRs *via* competitive ligand adsorption. The NPT and MBA ligands (Fig. 4E), both of which possess a thiol group with strong affinity to Au,[59–61] were used as competitive ligands to functionalize the surface of AuNRs. Apparently, the competition between these two ligands and their assembly on the surface of Au due to the different π–π stacking[62] is critical for the MOF selective growth. However, it is difficult to identify the phase segregation of these two ligands on the surface of AuNRs, as the ligand molecules are so small, and their chemical structures are quite similar to each other. It is important to note that the absorption of metal ions from the MOF only interacts with the MBA ligand, since it is the only one that has an exposed COOH group; therefore, the way the MOF structure surrounds the AuNR will depend on the proportion used for these two ligands in the reaction with Au.

3.6 Polyvinylpyrrolidone (PVP)

(i) Zhou *et al.*[45] proposed the PVP as a surface ligand covering AuNRs, and this product was prepared in deionized (DI) water overnight at r.t. However, the PVP-coated AuNR was then added to a *N*,*N*-dimethylformamide (DMF) solvent, because it exhibited high sterical stability, so it remained well dispersed. This ligand is electron-rich and is easily functionalized onto a Au

metal surface through the electronic pair of oxygen of the carbonyl group belonging to the pyrrolidone ring[63,64] (Fig. 4F). It was suggested that the PVP layer on the AuNR surface not only stabilizes the nanoparticles, but also interacts strongly with metal nodes *via* coordination interaction for subsequent nucleation and growth of porphyrin MOF (4) shell (based on Zr and porphyrin). To confirm this, free PVP was added into the reaction solution in a control experiment. The results indicated that only some nanoparticles were coated with a MOF shell, and there were three types of NPs in the final reaction mixture: (i) MOF nanorods, (ii) AuNRs, and (iii) AuNR@MOF. It demonstrated that the interaction between the PVP-coated AuNRs and metal nodes was inhibited by the competitive binding of free PVP.

(ii) Turner and Murphy[35] also used a PVP ligand that helps promote the growth of the ZIF-8 (2) MOF shell through its adsorption with the metal ions of the MOF. During the synthesis, AuNRs were stirred gently in nanopure water. Next, PVP in MeOH was prepared and added into a flask with Au and the solution was stirred gently again. The AuNRs were purified by centrifugation and were redispersed in MeOH. The PVP-capped AuNRs were then used as a basis for the growth of the MOF shell.

(iii) Li *et al.*[44] CTAB-stabilized AuNRs were centrifuged to precipitate them. After removing supernatant, a MeOH solution of PVP was added into the AuNR suspension and sonicated into a homogeneous solution following stirring at r.t. Then, the PVP-stabilized AuNRs were collected by centrifugation and the sample was redispersed in MeOH. AuNR surfaces were exchanged with PVP to avoid the possible toxicity of cationic CTAB on cells and tissues, considering the application focus (killing or damaging cancer cells) once the desired hybrid nanosystem is generated and, because its good adsorption on AuNRs makes the ZIF-8 (3) MOF grow around Au. All the above-mentioned ZIF-8 MOFs are based on the Zn metal center and methylimidazole as linkers.

(iv) In the work carried out by Liu *et al.*[46] the plasmon was encapsulated alone in a single copper oxide (Cu_2O) shell. In a typical synthesis, the NP stabilizer PVP ($M_w = \sim 55\,000$) was fully dissolved in a copper nitrate ($Cu(NO_3)_2$) aqueous solution under vigorous magnetic stirring. Then a AuNR solution was quickly injected, followed by the immediate introduction of a hydrazine hydrate ($N_2H_4 \cdot H_2O$) aqueous solution, a reducing agent that was probably added to prevent Au oxidation. Typically, the color changes to greenish yellow, indicating the formation of the Cu_2O shell. The reaction mixture was kept stirring, and the product was collected by centrifugation. Subsequently, the AuNRs were washed with EtOH and DI water to remove excess PVP, redispersed in benzyl alcohol (BnOH), and stored in a refrigerator at 4 °C. Apart from keeping the AuNRs protected from possible aggregation and dissolution in the reaction solution directing the growth of HKUST-1 (2) MOF crystals, the Cu_2O shell causes a gradual release of Cu^{2+} metal ions during the MOF synthesis acting as metal ion source. It is known that Cu_2O nanocrystals can undergo oxidative dissolution in a mildly acidic solution following the pathway $2Cu_2O + O_2 + 8H^+ \rightarrow 4Cu^{2+} + 4H_2O$,[65] a condition that can be achieved by partial dissociation of the linker used later to synthesize the MOF structure. It is important to mention that the thickness of the Cu_2O shell could be tuned by adjusting the $Cu(NO_3)_2$ concentration. Furthermore, multiple NPs can be encapsulated in a single Cu_2O shell which is an advantage.

3.7 Shell of SiO_2

According to a published article by Guo *et al.*[37] the AuNRs was initially capped with a mesoporous silica nanostructure (MSN). It was synthesized by an oil–water biphasic reaction approach. Typically, a cetyltrimethylammonium chloride (CTAC) surfactant was used to avoid aggregation,[66] and tetraethylammonium (TEA) was dissolved in DI water and also mixed with a AuNR suspension in water. The reaction solution was stirred at 60 °C, followed by the addition of 3-(mercaptopropyl)trimethoxysilane (MPTMS) in an EtOH solution. Afterward, tetraethoxysilane (TEOS) dissolved in cyclohexane (C_6H_{12}, immiscible with water) is slowly added to the upper layer of aqueous solution and reacted at 60 °C. Finally, the AuNR-MSN obtained was washed by centrifugation. The surfactants were removed by repeated reflux in an EtOH–HCl solution at 70 °C. To prepare the AuNR surrounded by the MOF, the AuNR-MSN was first reacted with 3-aminopropyl triethoxysilane (APTES) in EtOH to obtain AuNR-MSN-NH_2, and then it was dispersed in dimethyl sulfoxide (DMSO) and reacted with maleic anhydride ($C_4H_2O_3$) to generate AuNR-MSN-COOH, which was collected and purified by centrifugation (Fig. 4G). The metal source initially added allows the start of growth of the Fe-based MOF (5) interacting with the COOH group exposed. Unlike silica (Si), MOFs have the advantages of being biodegradable,[67–70] which is favorable in nanomedicine, also have lower toxicity although this varies depending on their chemical composition and their physical–chemical properties, including their colloidal and chemical stability[71] and can adsorb a wide variety of species between their nanopores, giving way to diverse applications.

4. MOF growth methodology around AuNRs

Once the AuNR is capped with a surface ligand, the growth of the MOF is generated by adding a metal center and a linker. To produce a AuNR@MOF nanohybrid following the general strategy A (Fig. 1), different synthetic methodologies have been carried out, including LbL, microwave, solvothermal and stirring at r.t. or stirring with temperature (Fig. 5).

Additionally, it has been found that the addition of an appropriate amount of a modulator (*e.g.,* acetic acid, amino acids, and benzoic acid) can influence the formation of its crystalline structure.[72,73] Hence, the addition of some types of modulators is common. Below we show in detail the synthesis conditions, synthetic methodologies, and morphology characteristics of the MOF shells around the AuNRs (Table 2).

4.1 Layer-by-layer (LbL)

4.1.1 HKUST-1 (1). The $Cu(OAc)_2$ metallic source added acts as a Paddle wheel once it interacts with exposed end COO^-

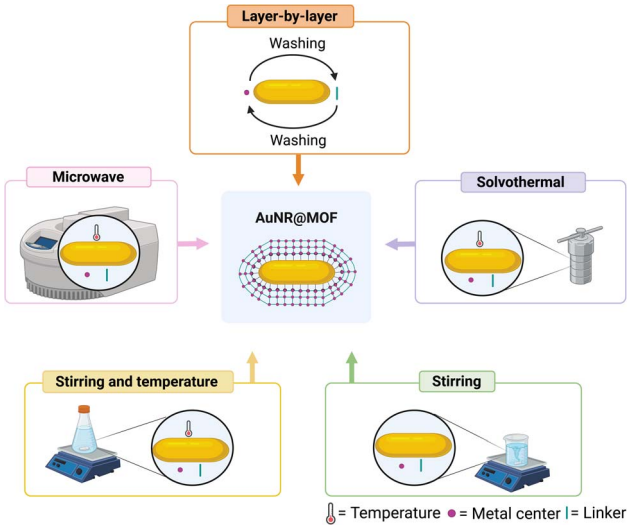

Fig. 5 Schematic of the MOF growth methodologies for the formation of AuNR@MOF nanohybrids.

of MUA, allowing the formation of the first $\frac{1}{2}$ layer of the MOF by the LbL methodology in an EtOH solvent at r.t.[36]

Then the conjugate base of the 1,3,5-benzenetricarboxylate (BTC) organic linker was added into an EtOH solution, that is, a tetramethylammonium salt of 1,3-benzenetricarboxylate (TMABTC, Fig. 6A), which gives negative charges to BTC (Fig. 7), thus completing the first layer. During this synthesis, it has been shown that controlling the surface charge during synthesis can prevent aggregation. Centrifugation must also be controlled during washing, since if too much speed is applied, aggregation can occur. Here 24 layers were obtained in total, resulting in a MOF thickness of 6.1 ± 0.8 nm, which covers the AuNRs (Fig. 8A).

As this method deposits the components of the MOF in a truly LbL fashion, it allows for subnanometer control over the shell thickness. Along with, it was demonstrated that in order to synthesize MOF shells, it was crucial to functionalize the surface of AuNRs with ligands onto which the MOF precursors adsorb strongly.

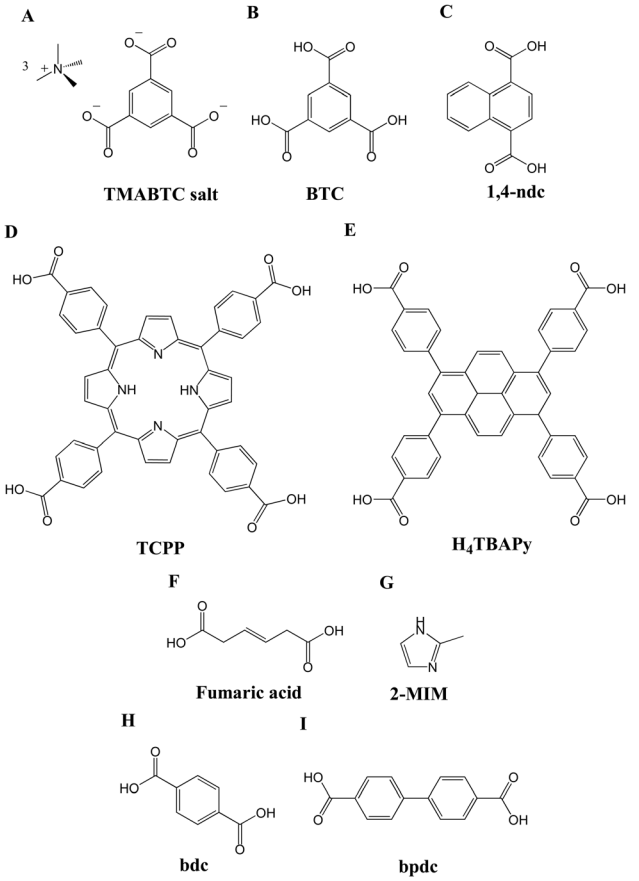

Fig. 6 Chemical structures of the organic linkers: (A) TMABTC salt; (B) BTC; (C) 1,4-ndc; (D) TCPP; (E) H_4TBAPy; (F) fumaric acid; (G) 2-MIM; (H) bdc; and (I) bpdc.

4.1.2 Fe-based MOF (5). Nanohybrid AuNR-MSN-MOF was also prepared by the LbL growth method.[37] First of all, AuNR-MSN-COOH was washed and dispersed in DI water by

Table 2 Morphology characteristics around AuNRs reported in the construction of AuNR@MOF nanohybrids

MOF name[a]	MOF thickness (nm)	Pore size (nm)	Ref.
HKUST-1 (1)	2, 3, 4, 5, 6	—[b]	36
MOF (5)	—[b]	—[b]	37
[Al-(OH)(1,4-ndc)]$_n$	—[b]	—[b]	38
MOF (2)	8.2 ± 2.3 (4 h) 14.8 ± 1.6 (6 h)	1.6 ± 0.3	39
MOF (3)	8.1 ± 2.3 (4 h) 13.2 ± 1.6 (6 h)	1.6 ± 0.3	40
NU-901	—[b]	—[b]	41
MIL-88 (A)	—[b]	—[b]	42
ZIF-8 (1)	—[b]	—[b]	43
ZIF-8 (2)	39 ± 8 end × 43 ± 6 side	1.1, 1.5 and 2.8	35
ZIF-8 (3)	—[b]	1.74	44
MOF-5	—[b]	0.417	14
MOF (4)	40 to 80	1.2 and 3.0	45
HKUST-1 (2)	—[b]	—[b]	46
MOF (1)	—[b]	—[b]	13

[a] Articles that presented the same names of MOFs are listed with different numbers in parentheses to distinguish each of them. [b] Not reported.

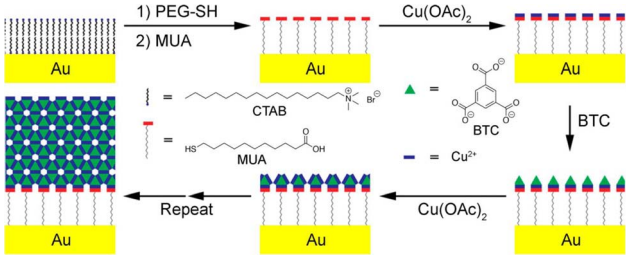

Fig. 7 Synthetic conditions used for LbL coating of AuNRs with HKUST-1 (1). Reproduced from ref. 36. Copyright 2018 ACS Publications.

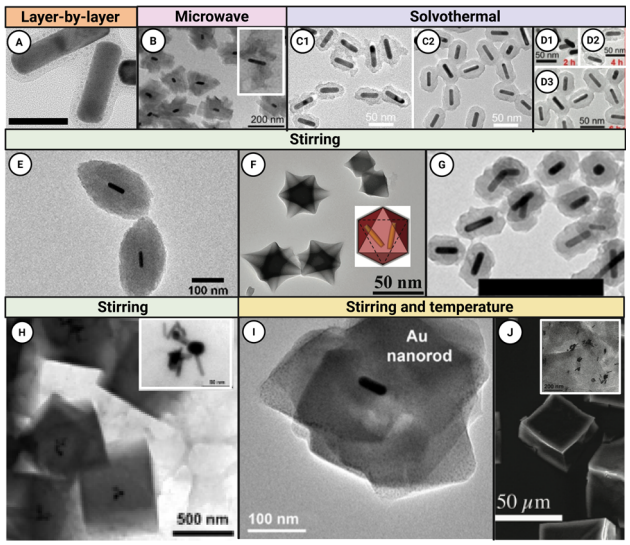

Fig. 8 Schematic of the growth of MOFs on AuNRs. TEM image of: (A) AuNR@HKUST-1 (1)-coated AuNRs after 24 layers. Reproduced from ref. 36. Copyright 2018 ACS Publications. (B) AuNR@[Al-(OH)(1,4-ndc)]$_n$. Reproduced from ref. 38. Copyright 2013 ACS Publications. (C) AuNR@MOF (2) collected after 4 h (C1) and 6 h (C2) of reaction. Reproduced from ref. 39. Copyright 2017 ACS Publications. (D) AuNR@MOF (3) collected after 2 h (D1), 4 h (D2) and 6 h (D3) of reaction. Reproduced from ref. 40. Copyright 2018 Wiley Online Library. (E) AuNR@NU-901. Reproduced from ref. 41. Copyright 2019 ACS Publications. (F) AuNR@MIL-88 (A) Reproduced from ref. 42. Copyright 2017 Wiley Online library. (G) AuNR@ZIF-8 (2). Reproduced from ref. 35. Copyright 2021 ACS Publications. (H) AuNR@MOF-5. Reproduced from ref. 14. Copyright 2013 ACS Publications. (I) Yolk-shell AuNR@HKUST-1 (2) petalous heterostructure. Reproduced from ref. 46. Copyright 2014 ACS Publications. (J) AuNR@MOF (1). Reproduced from ref. 13. Copyright 2011 ACS Publications.

ultrasound. Then, a $FeCl_3$ solution was added dropwise under ultrasonic conditions and the mixture was further stirred at r.t. The solution of Fe^{3+} coordinated with AuNR-MSN-COOH was collected and washed by repeated centrifugation. Subsequently, the above-mentioned product was dispersed in an ethanol solution containing BTC and the reaction was continued at r.t. before centrifugation and washed to collect the product. Unlike the previous example (Fig. 6A), in this synthesis the BTC linker (Fig. 6B) is not found in salt form at the time of adding the metallic source, in this case the Fe_3^+, which does not prevent subsequent interaction with this metal.

Next, hyaluronic acid (HA) was completely dissolved in water, into which the previously obtained nanohybrid was introduced and reacted overnight, to improve its biocompatibility.

After repeated centrifugation steps, the HA-wrapped AuNR-MSN-MOF was obtained and denoted as AuNR-MSN-MA. After three repeated MOF (5) growth processes, the AuNR-MSN-MOF was obtained and purified by centrifugation.

4.2 Microwave

4.2.1 [Al(OH)(1,4-ndc)]$_n$. Here an amorphous alumina layer was deposited onto the AuNR-S-$(CH_2)_2$CO-NH-PEG-OH surface by a sol–gel process.[38] Initially, the PEGylated AuNRs contained in water were mixed with a dry ethanolic solution of aluminum-tri-*sec*-butoxide ($Al[OCH(CH_3)C_2H_5]_3$) as an aluminum precursor. Mineral polymerization was initiated by the addition of a small amount of water, which led to AuNRs embedded within a hydrated amorphous alumina matrix. Notably, no well-defined core–shell AuNR@alumina nanostructures were observed on TEM pictures (superimposed in Fig. 8B), but it was believed that the irregular alumina coating observed on these pictures was an artifact originating from the preparation of the TEM grids. Indeed, at r.t. and under the experimental conditions, the amorphous alumina produced in a water/EtOH solution is most probably composed of soluble aluminum hydroxide oligomers attached to the PEG chains through the formation of a hydrogen-bonding network between the ethylene oxide units of the PEG chains and the hydroxide groups of the alumina species.[74] Consequently, the observed irregular alumina coating likely originated from the collapse and further condensation of the soluble alumina species during the drying step of TEM grid preparation. Then, the linker 1,4-naphthalenedicarboxylic acid (1,4-ndc, Fig. 6C) was added to the freshly washed AuNR@alumina suspension, and the resulting mixture was treated under microwave conditions at 180 °C within 60 s generating a MOF (which in some articles is also called porous coordination polymer (PCP)) nucleation on the AuNR surface. This resulted in the formation of discrete particles with well-defined core–shell composites called AuNR [Al(OH)(1,4-ndc)]$_n$ (Fig. 9). Thus, the surface of AuNRs acts as a starting point for the MOF heterogeneous nucleation.

The utilization of alumina-modified AuNRs as reactive seeds was the key point to precisely controlling the localization of MOF crystallization onto the Au surface. This strategy directly derives from a dissolution-recrystallization process, called coordination-replication, which was established in a previous study for the formation of MOF architectures.[75]

This process was based on the pseudomorphic replacement of a metal oxide phase that is out of equilibrium by a more stable MOF in the presence of a multitopic organic linker. The preservation of the shape and dimension of the phase was guaranteed by a precise coupling between kinetics of the metal oxide dissolution and kinetics of MOF crystallization.

If we compare this microwave methodology with the previous LbL, we can see that the reaction time to generate the MOF around the plasmon is noticeably shorter (which means

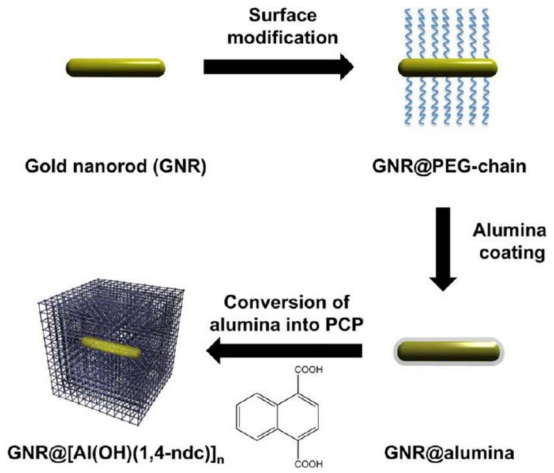

Fig. 9 Schematic of the synthesis of AuNR@[Al(OH)(1,4-ndc)]$_n$ core–shell composites. Reproduced from ref. 38. Copyright 2013 ACS Publications.

that it is less laborious), considering that the LbL methodology can last for days, which will depend mainly on the incubation time and washed after adding the linker and the metal center and, the thickness of the MOF that is intended to be obtained, taking into account that with this methodology there is a control of the thickness, which will depend on the number of layers to be generated.

4.3 Solvothermal

4.3.1 Porphyrin MOF (2). A porphyrin MOF was fabricated by a solvothermal method using the AuNR surface carboxylated by SAM with LA as crystal nuclei. In this synthesis process, the modified-AuNR was dispersed in DMF by sonication and $ZrOCl_2 \cdot 8H_2O$ was added. The mixture was heated to 90 °C. Then, tetrakis(4-carboxyphenyl)porphyrin (TCPP, Fig. 6D) and benzoic acid[39] were added and stirred at 90 °C. After the reaction finished, the composites were collected *via* centrifugation followed by washing with DMF, triethylamine in EtOH, and EtOH successively. The nucleation and controllable growth of MOFs on the AuNR nanostructure surface can be driven by the coordination interactions between functional groups of the nanostructure surface and Zr nodes (generated in the reaction once the metal source $ZrOCl_2 \cdot 8H_2O$ was added). It was confirmed that porphyrin MOF surrounds the AuNR surface using TCPP as the organic linker and Zr^{4+} as the metal node under solvothermal conditions (Fig. 8C). Moreover, the localized MOF nucleation growth on the surface of AuNR can be controlled by the reaction time, leading to the formation of well-defined core–shell composites. In fact, the TEM image of AuNR@MOF shows that the thickness of the MOF shell was about 8.2 ± 2.3 nm after the MOF-formation reaction time at 4 h (Fig. 8C1). Increasing the reaction time to 6 h gave rise to a thickness of 14.8 ± 1.6 nm (Fig. 8C2).

4.3.2 Porphyrin MOF (3). First, functionalized AuNRs were washed twice with DMF to remove water. Functionalized AuNRs were suspended in DMF and then mixed with a TCPP tetratopic linker, benzoic acid and $ZrOCl_2 \cdot 8H_2O$. The mixture was stirred at r.t. and then heated to 90 °C. After cooling down, the core–shell composites were collected *via* centrifugation followed by washing with DMF, triethylamine in EtOH, and EtOH successively. Localized MOF nucleation growth on the surfaces of AuNRs leads to the formation of the core–shell composites. The chosen porphyrinic MOF is $Zr_6(TCPP)_{1.5}$, which is composed of a 6-connected Zr_6 cluster ($Zr_6O_4(OH)_4(H_2O)_6(OH)_6(COO)_6$) and a tetratopic linker.[40] Additionally, the thickness of the MOF shell on the surfaces of AuNRs can be controlled by the MOF growth time at 2, 4 and 6 h of reaction (Fig. 8D1–8D3).

Like the LbL methodology, the solvothermal methodology also allows the thickness of the MOF to be controlled around the plasmon, which depended on the reaction time. Like the microwave reaction, these have required less synthesis time compared to the LbL ones, which represents an advantage.

4.4 Stirring

4.4.1 NU-901. After obtaining the AuNRs, core–shell crystallites were synthesized (Fig. 8E) following a two-step procedure adapted from Noh *et al.*[41,76] Here, Zr clusters were first formed at high temperatures and then isolated. It is composed of 8-connected $Zr_6(\mu_3\text{-}O)_4(\mu_3\text{-}OH)_4\text{-}(H_2O)_4(OH)_4$. The isolated clusters were dispersed in a mixture of DMF and acetic acid. The stabilized PEG-AuNRs were added to this suspension (Fig. 10), resulting in a deep red mixture of DMF and acetic acid. Next, under vigorous stirring, the tetratopic linker 1,3,5,8-(*p*-benzoate)pyrene (H_4TBAPy) (Fig. 6E) was added in DMF. A dark red precipitate formed was removed by centrifugation, washed extensively using DMF, and solvent-exchanged to ketone.

Initial attempts to create core–shell structures using PVP-capped AuNRs, with a more conventional NP@MOF encapsulation agent,[77] were unsuccessful and resulted in AuNR aggregation outside the NU-901 crystallites. Similarly, AuNRs functionalized with MUA aggregated during the synthesis and were not encapsulated by the MOF. It is suggested that the PEGylated AuNRs generate the MOF growth, presumably due to

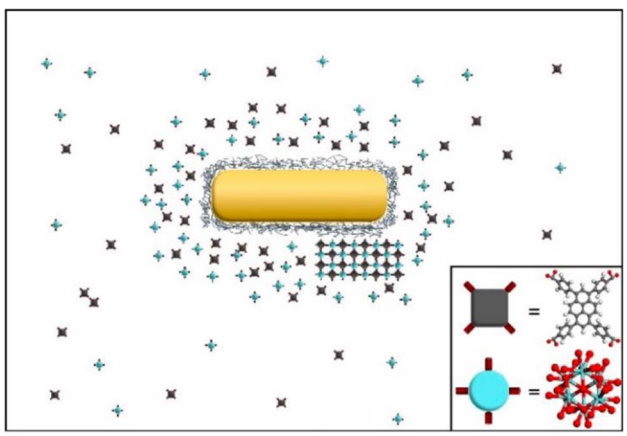

Fig. 10 Interactions between PEG surrounding the AuNR and MOF precursors, which are Zr-cluster (calypso) and H_4TBAPy-linker (gray). Reproduced from ref. 41. Copyright 2018 Wiley Online Library.

interactions (dispersion forces, dipole–dipole interactions, *etc.*) between the MOF precursors and PEG due to its hard oxygen and soft ethylene moieties. These interactions may increase the local concentration of the precursors on the surface of the AuNRs, making a nucleation event kinetically more favorable. The model has two additional features in the nucleation and growth phase: (i) favorable interactions between the PEGylated AuNRs and the MOF precursors, which lower the nucleation threshold locally on the AuNRs, and (ii) at a critical low concentration of H_4TBAPy during the growth phase, the topology changes from scu-topology NU-901 to csq-topology, resulting in the less dense NU-1000 structure. In both structures, the Zr-clusters have 8 loosely H_2O/OH-coordinated sites as possible catalytic centers.

4.4.2 MIL-88 (A). Ionic liquid/microemulsion was used to encapsulate the COOH-terminated AuNRs as the core and control the growth of the MOF. The MOF-optimized synthesis was performed as follows: first, a mother MOF solution was prepared with $FeCl_3 \cdot 6H_2O$, a fumaric acid linker (Fig. 6F)[42] dispersed in an emulsion of PEG ($M_w = 3500$ g mol^{-1}), 1-butyl-3-methylimidazolium hexafluorophosphate ($BmimPF_6$) and DMF.

The mixture was subject to vigorous magnetic stirring at r.t. for homogenous dispersion. Then, the solution was heated to 80 °C and maintained at this temperature during the addition of the COOH-terminated AuNRs. Next, the solution was quickly cooled down until crystallization. The mixed solution was kept under constant incubation, centrifuged and then washed with EtOH and DI water. During the encapsulation of AuNRs with ionic liquid/microemulsion, two AuNRs were supposed to be assembled as the core in the microemulsion due to the intrinsic property and the size of microemulsion, as well as the lower ΔG that maintains the assembly of two AuNRs in the microemulsion. Indeed, in this case, almost all the nanostructures contained two AuNRs as the core. This nanostructure has a high monodispersity and homogeneity and a well-defined star-like morphology (Fig. 8F). These core–shell nanostructures were synthesized through controllable growth of the MOF shell on the surface of Au.

In order to improve the biocompatibility and stability of MOFs, nanocrystals were modified with PEG chains (M_w = 3500 g mol^{-1}) having only one terminal reactive group (carboxyl) after the synthesis process, leading to the formation of a superficial PEG "brush" that protected the nanostructure from aggregation. ζ-potential measurements clearly indicated that neutral PEG chains were located on the surface of the nanoparticles. The ζ-potential values of uncoated MIL-88 (−17 mV) were shifted to almost neutral values (−3 mV) in the case of PEGylated MIL-88 (A). The nanostructure obtained after modification was called AuNR@MIL-88 (Fe) (Fig. 11).

4.4.3 ZIF-8 (1). Zinc nitrate ($ZnNO_3$) and 2-methylimidazole (2-MIM) (Fig. 6G) were used as precursors for the growth of this MOF on AuNRs self-assembled with NPT and MBA.[43] Interestingly, for NPs@MOF, three types of structures can be obtained in general, they are: (i) eccentric core–shell, (ii) Janus nanohybrids (absence of centro-symmetry demonstrates higher diversity and complexity, particularly with Janus structures) and (iii) concentric core–shell (uniform shell or granular domains in colloidal systems)[78,79] (Fig. 12).

To synthesize eccentric core–shell Au-ZIF-8 nanohybrids, an Au solution was concentrated by centrifugation. After the removal of supernatants, the residual NPs were re-dispersed into MeOH. MBA and NPT in MeOH, with a ratio of 1 : 1, were used as competitive ligands and added into the Au solution under mild stirring. After the reaction, $ZnNO_3$ was added to the solution. The above solution was stirred to make sure that Zn^{2+} ions adsorbed onto the surface of Au.

Subsequently, a 2-MIM linker in a MeOH solvent was injected into the mixture and the solution was stirred overnight. To isolate the product, the reaction mixture was centrifuged and the supernatant removed. The resulting nanohybrid particles were dried in a vacuum oven overnight.

To prepare Janus AuNR-ZIF-8 nanohybrids, the amount of ligands added into the solution was changed, so that the mixture contains NPT and MBA in a ratio of 3 : 1, respectively, with all other conditions unchanged. Thus, the eccentric core–shell and Janus nanohybrid structures, both with a hexagonal morphology of the MOF, were a result of NPT and MBA adsorption on AuNRs. As explained above, the MBA carboxylic groups are exposed, which improves the hydrophilicity of the Au surface. Consequently, the MOF metal precursors, Zn^{2+} ions, were fully adsorbed on the Au surface *via* electrostatic interaction with MBA carboxylic groups. In contrast, Zn^{2+} ions were unable to adsorb on the AuNR surfaces self-assembled with NPT due to its high hydrophobicity after functionalization. It explains why a more eccentric morphology is obtained upon increasing the NPT concentration to a ratio of 3 : 1, forming Janus nano-hybrids with AuNRs. Thus, the molar ratio of these competitive ligands determines the morphology of these nanohybrid products. In summary, the formation of eccentric core–shell and Janus nanohybrids can be only achieved by adding dual ligands with different surface affinities to the MOF precursors.

4.4.4 ZIF-8 (2). The PVP-capped AuNRs were then used as a core for the growth of MOF shell.[35] Initially, PVP-capped AuNRs were mixed with 2-MIM prepared in MeOH. The solution was stirred, and then, $ZnNO_3 \cdot 6H_2O$ in MeOH was added. Afterwards, the ZIF-8-coated AuNRs were centrifuged. The resulting nanoparticles (Fig. 8G) were redispersed in MeOH as well, washed again, and then slowly washed to help separate any free MOF particles. The nanoparticles were stored in MeOH until use. Turner and Murphy suggested that PVP helps promote the growth of the ZIF-8 shell through its adsorption with Zn ions that are part of the MOF metallic center.

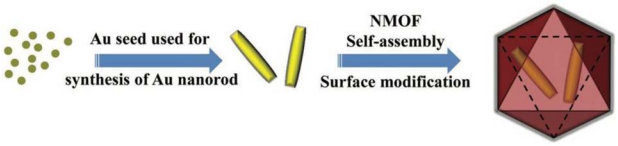

Fig. 11 Schematic of the synthesis of AuNR@MIL-88 (Fe) nanostars. Reproduced from ref. 42. Copyright 2017 Wiley Online library.

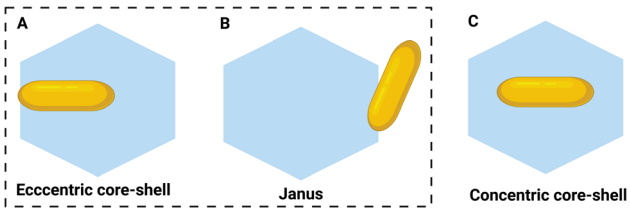

Fig. 12 Schematics of the growth of different types of AuNR@ZIF-8 hybrid nanostructures determined by ligand competition: (A) eccentric core–shell; (B) Janus nano-hybrids; and (C) concentric core–shell (it was not synthesized in this study).

4.4.5 ZIF-8 (3). At r.t., PVP-stabilized AuNRs and 2-MIM were mixed and stirred in a MeOH solution. Then, a solution of $Zn(NO_3)_2 \cdot 6H_2O$ in MeOH was added into the mixed solution. Later, the final product was obtained by centrifugation, washed with MeOH and dried at r.t.[44]

4.4.6 MOF-5. Interestingly, in this work, a supersaturated mother solution of this MOF was first prepared. Samples of phthalic acid (bdc) used as the linker (Fig. 6H) and $Zn(NO_3)_2 \cdot 6H_2O$ as the metal center were thoroughly dissolved in *N*,*N*-diethylformamide (DEF) with ultrasonication.[14] The solution was heated to 90 °C and kept at this temperature until the beginning of crystallization. The supersaturated mother solution was filtered and cooled down to r.t. MUA-capped AuNR was added into this MOF mother solution, and the mixed solution was incubated at r.t. The solution became cloudy after a few minutes, suggesting the formation of MOF-5 crystals. We can observe the TEM images of the AuNR@MOF-5 nanocrystal (Fig. 8H) and of various AuNRs within a cubic MOF crystal (superimposed in Fig. 8H). The obtained nanocrystal was collected by centrifugation, which was redispersed into organic solvents such as DEF and DMF. It should be noted that in the stirring and LbL methodology, the MOF surrounding the plasmon was synthesized at r.t., which is an advantage since the plasmon and the components chosen to form the MOF could be unstable at high temperatures. Moreover, it is interesting that this is the methodology with which the largest quantity of AuNR@MOF nanohybrids have been synthesized.

4.5 Stirring and temperature

4.5.1 Porphyrin MOF (4). The growth of a MOF shell on PVP-coated AuNRs was conducted at 90 °C in DMF, containing PVP-coated AuNRs, TCPP, $ZrOCl_2 \cdot 8H_2O$, benzoic acid, and trace amounts of water.[45] The resulting purple solids were collected by centrifugation and re-dispersed in DMF. It was suggested that the PVP on the AuNR surface not only stabilizes the NPs in the growth solution, but also interacts strongly with Zr atoms in Zr_6 nodes *via* coordination interaction for subsequent nucleation and MOF growth with rod-shaped morphology around the AuNR, which was collected after 0, 4, 6, 8 and 12 min, and 3 h of reaction.

4.5.2 HKUST-1 (2). The linker that causes the Cu_2O shell oxidative reaction leading to the gradual release of the Cu^{2+} metallic source is the BTC. In this synthetic approach, the linker also serves as the etching reagent in addition to being the linker and the oxidizing species. In the synthesis process, BTC was added into a mixture of BnOH and EtOH and then sonicated to afford a homogeneous solution. Subsequently, AuNR@Cu_2O core–shell NPs were added to BnOH, thoroughly mixed by shaking, and then allowed to react at 80 °C. The product was collected by centrifugation, washed several times with MeOH, and finally redispersed in the same solvent. In the process, Cu_2O shell encapsulates the plasmon during the synthesis into Yolk-shell HKUST-1 (2) petalous heterostructures (Fig. 8I) without aggregation owing to the low ionic concentration.[46]

4.5.3 Zn-based MOF (1). Initially, MUA-capped AuNRs redispersed in DEF were mixed with DEF containing 4,4′-biphenyldicarboxilate (bpdc) (Fig. 6I) and $Zn(NO_3)_2 \cdot 6H_2O$ at 80 °C (direct growth of $Zn_4O(bpdc)_3$).[13] After incubation of the mixture at 80 °C, the supernatant turned its color from purple to light yellow, and purple cubic crystals were obtained. The crystal morphology was characterized by well-defined cubic crystals 20–120 μm in width. The smooth crystal surface and the purple color indicate that AuNRs were incorporated inside MOFs because the virgin MOF was intrinsically transparent. The TEM image of AuNR@MOF (1) showed that several partially aggregated AuNRs (superimposed in Fig. 8J) were embedded homogeneously in a cubic MOF crystal (Fig. 8J).

As mentioned above, applying temperature to obtain Au plasmon-based nanohybrids and MOFs can be a disadvantage. However, it has been shown that this methodology also allows controlling the thickness of the MOF by modifying the reaction time, which can be an advantage depending on the desired application of the nanohybrid.

In summary, the LbL methodology has some advantages over others, and this is because there is a greater control over the thickness of the MOF around NPs. The thickness of the coordination polymer is an important factor since if the focus of the application is to absorb or transport molecules or drugs, for example, it could be convenient to generate a greater quantity of nanopores that allow increasing their concentration if required. Yet, it also has some disadvantages since it is a longer and more laborious process because each time the metal center and the linker are added, it is necessary to use an incubation period and several washing processes to avoid the formation of MOFs apart from the hybrid nanosystem. It is important to highlight that the centrifugation speed and time must also be controlled during washing to avoid aggregation. Besides, it is carried out at r.t., which avoids possible aggregation and/or decomposition of the nanosystem, for instance.

Although the other methodologies are normally faster and less laborious, there is no greater control of the MOF thickness and higher temperatures could also be required (depending on the solvent to be used), which limits the reaction to using components (*e.g.,* NPs, source ligands, MNs, metal sources, and linkers) that do not decompose at high temperatures.

5. AuNR@MOF applications

The characteristics of the AuNR and MOF together enable AuNR@MOF nanostructures to be used in molecular and drug

uptake/release, NIR-triggered photothermal and chemotherapy to damage cancer cells, biomedical imaging and detection of analytes by SERS, to give some examples (Fig. 13). However, to give them a particular application, there are important factors to consider, among which are the following ones: (i) environment, (ii) MOF pore size, (iii) nanostructure size, (iv) biocompatibility and (v) biodegradability. These nanostructures are more stable in certain solvents, temperatures, and pH than in others, which will depend on the characteristics of AuNRs and MOFs that surround it, which is very important if we intend to use them in either *in vivo* or *in vitro* experiments, since they can be exposed to aggregation or decomposition.

As is known, MOFs are coordination compounds characterized by being nanoporous, which allows them to accommodate different guests (*e.g.*, molecules, proteins and drugs). These pores can be of different sizes, which is decisive when selecting the type of guest that is intended to be accommodated between them. Furthermore, the host functional groups can be decisive to introduce guests into these pores, which will depend on the affinity that the MOF components have for them. Moreover, the AuNR@MOF size is relevant to biological applications, since nano-scale sizes are ideal, so that they can interfere at the cellular level, where the biocompatibility factor must also be considered. It should be noted that another feature of MOFs is that they can be biodegradable and, as has already been seen in some of the examples, they can also be built with essential metals, allowing toxicity levels to be reduced in biological applications.

5.1 Photothermal effects

To investigate the photothermal effect of AuNR-MSN-MA on cancer cell killing, murine breast carcinoma cell line 4T1 was incubated with this nanohybrid and irradiated by NIR.[37] At the same concentration of the nanohybrid, the cell death rate decreased with the increase in the power density of the NIR laser. In contrast, no appreciable damage was observed for cells exposed to NIR laser alone, suggesting the minimal side effect of applied laser. The killing effect can also be enhanced when the concentration of the nanostructure increases. In particular, the relative cell viability was only 13.8% for cells treated with 200 μg mL^{-1} AuNR-MSN-MA under laser irradiation. Therefore, the results confirm excellent biocompatibility and biodegradability, so it can be concluded that it is a promising nanoplatform for biomedical applications.

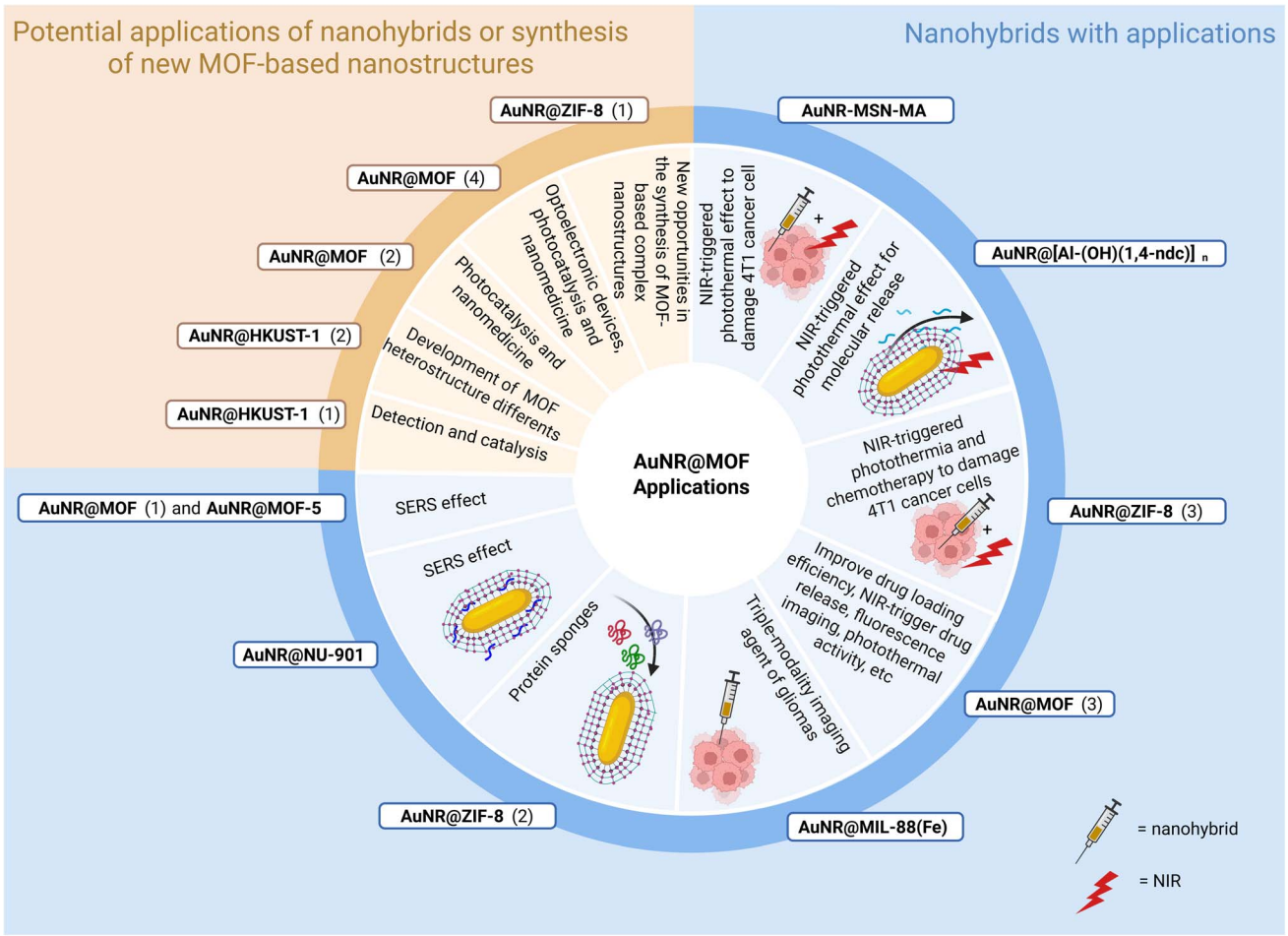

Fig. 13 Schematic of the potential applications of AuNR@MOF nanohybrids, potential synthesis of new MOF-based nanostructures, and the applications of AuNR@MOF nanohybrids that have been used to date.

The doxorubicin hydrochloride (DOX, medicine for the treatment of different types of cancer)-loaded AuNR-MSN-MA (DOX@AuNR-MSN-MA) was demonstrated with excellent target ability toward cancer cells. Accordingly, upon NIR laser irradiation, DOX@AuNR-MSN-MA also displays outstanding combined efficiency for killing the cancer cell *in vitro* and suppressing the tumor growth *in vivo*. Furthermore, AuNR-MSN-MA integrates tri-modal magnetic resonance/computed tomography/photoacoustic (MR/CT/PA) imaging into a single platform. The efficient *in vivo* MR/CT/PA imaging on tumor model was confirmed.

The fabrication of the AuNR@[Al-(OH)(1,4-ndc)]$_n$ composite involves the use of AuNRs as an optical switch and a MOF for controlled anthracene molecular release using NIR-light irradiation as an external trigger.[38] In summary, here a strategy was developed for controlling the molecular release from the MOF pores by combining the loading and unique guest stabilizing ability of the MOF with the photothermal properties of AuNRs. The photothermal conversion ability of the AuNRs acts as an optical switch that enables them to remotely release the guest molecules adsorbed within the MOF pores through an increase of molecular mobility. The release of anthracene under NIR light irradiation demonstrated the efficiency of this new molecular release system. This research also demonstrated the method for incorporating the core–shell composites into biocompatible polymethylglutarimide (PMGI) nanofibers known to be good cell-culture scaffolds.[80] Along with it, this system will offer the possibility to spatially control the molecular release and to integrate them into biological systems for future applications in the field of cell biology. Moreover, it can be anticipated that these MOF-based composites will be used as platform systems for the remote-controlled release of various relevant bioactive molecules to chemically stimulate living cells. The AuNR@ZIF-8 (3) nanohybrid[44] is a crystalline zeolitic imidazolate framework-8 (ZIF-8), which covers a single AuNR core for successful realization of synergistic photothermal and chemotherapy triggered by NIR light. Under NIR laser irradiation at 808 nm, these novel core–shell nanostructures show potential for effective synergistic chemo-photothermal therapy both *in vivo* and *in vitro*, confirmed by cell treatment and tumor ablation *via* intravenous injection on the 4T1 cells. Impressively, high DOX loading capacity followed by pH and NIR light dual stimuli-responsive DOX release can be easily implemented through the formation and cleavage of coordination bonds in the system.

In the case of the AuNR@MOF (3) nanostructure,[40] it was used as a delicate tunable core–shell composite which not only possesses NIR-trigger drug release but also can improve the drug loading efficiency, fluorescence imaging, reactive oxygen species (ROS) production and photothermal activity to achieve combined cancer therapy. It was further demonstrated that the camptothecin (CPT, medicine for the treatment of few types of cancers)-loaded AuNR@MOF nanohybrid shows distinctively synergistic efficiency for damaging the murine breast tumor 4T1 cells *in vitro* and inhibiting the tumor growth and metastasis *in vivo*. The development of this high-performance nanostructure will provide more perspectives for the design of versatile nanomaterials for biomedical applications.

5.2 Biomedical imaging

The modified nanoparticles named AuNR@MIL-88 (Fe) served as triple-modality imaging agents.[42] These core–shell nanoparticles simultaneously possess CT imaging enhancement and PA imaging optical properties and the T_2-weighted MR imaging property for *in vivo* and *in vitro* experiments. These nanoparticles exerted low cytotoxicity and showed high-enhancement CT, MR, and PA imaging for *in vivo* studies of gliomas in mice. Both CT and MR images showed a clear structure with high depth of penetration. They further demonstrated utility for PA imaging of gliomas with clear detection, high spatial resolution, and high contrast. Remarkably, both *in vivo* and *in vitro* experiments demonstrated that the MOF exhibited high performance in various diagnosis and imaging methods, especially potentially allowing decreased levels of exposure of stroke patients to CT imaging radiation. Although the research is still in its infancy, as demonstrated in this work, researchers believe that it provides opportunities for advanced triple-modality molecular imaging, from preclinical to clinical investigation to determine timely diagnosis of gliomas in patients.

5.3 Molecular adsorption

As AuNPs have become more common in many technological sectors, much research has focused on the biological and environmental fate of these materials.[81–83] A more complete understanding of how AuNPs interact with biomolecules and individual cells is expected to inform our understanding of their fate in entire organisms and ecosystems.[84,85] Moreover, a deeper understanding will greatly improve the design of NPs for therapeutics, imaging agents, and other biologically relevant applications. When colloidal nanomaterials are exposed to a complex biological environment, they acquire biomolecules on their surfaces to form the so-called protein coronas. Indeed, porous nanomaterials such as MOFs offer the opportunity to sequester biomolecules and/or control their surface orientation. Hence, in the AuNR@ZIF-8 (2) nanomaterial study, it was compared to ZIF-8 nanoparticles as potential protein sponges to adsorb several common proteins such as lysozyme, beta-lactoglobulin-A (BLG-A), and bovine serum albumin (BSA) and potentially control their orientation on the surface. Of the three proteins investigated, the smallest protein that was also electrostatically favorable, BLG-A, was the most adsorbed to the surface of ZIF-8. Nevertheless, AuNR@ZIF-8 adsorbed a higher amount of proteins than ZIF-8. For the set of proteins and nanomaterials in this study, all protein-surface interactions were exothermic, as judged by isothermal titration calorimetry. Protein display at the surfaces was determined from limited proteolysis experiments, and it was found that protein orientation was dependent both on the nature of the nanomaterial surface and on the nature of the protein, with lysozyme and BLG-A showing distinct molecular positionings.[35]

5.4 SERS effect

The NP@MOFs provide a unique opportunity to harness the optical properties of noble metal nanoparticles such as AuNRs for integrated spectroscopy probes. Based on the above-mentioned facts, the functionality of the AuNR@NU-901 nanohybrid was demonstrated by using the AuNRs as embedded probes for selective SERS, which enhances the characteristic molecular Raman signal by multiple orders of magnitudes.[41,86–88] This nanostructure was able to both take-up or block molecules from MOF pores, thereby facilitating highly selective sensing at the AuNR ends. In this investigation, the SERS capability of AuNR inside the MOF crystallites was utilized by infiltrating the MOFs with thiolated aromatic analytes such as 4′-mercaptobiphenylcarbonitrile (BPTCN) and biphenyl-thiol (BPT). The resulting spectra clearly contained both MOF peaks and analyte peaks, indicating successful adsorption. As a negative control, the nanostructure was incubated with a bulky polymer (thiolated polystyrene (PST-SH; $M_w = 5000$ g mol^{-1})), which was subsequently blocked by the porosity of the MOF and not detected by the AuNRs. This proof-of-principle work sets the stage for both advanced MOF synthesis and embedded probe spectroscopy using the AuNRs for selective SERS and provides a new capability for MOF plasmonics.

It has also been demonstrated that the fabrication of the AuNR@MOF (1)[13] composite crystals was successfully used for monitoring *in situ* diffusion of DEF and trichloromethane ($CHCl_3$) guest molecules from MOF crystals by SERS. It was hypothesized that this nanohybrid should be suitable for studying the transport phenomenon in MOF nanopores, which significantly contributes to its design function.

The AuNR@MOF-5 ref. 14 nanostructure was also used for SERS applications. It was dispersible and stable in organic solvents (DEF and DMF) and demonstrated to be a reproducible SERS material for size-selective detection of some pyridine derivatives, among which are pyridine (Py), 2,6-bi-phenylpyridine (BPPy), and poly(4-vinylpyridine) (PVPy), as analytes, in DMF. In this nanosystem, these derivatives were proved to diffuse through nanopores of MOF-5 shells and interact with the surface of AuNR encapsulated in MOF nanocrystals. Small molecules such as Py and BPPy were able to diffuse into the nanopore of the MOF-5 shell and interact with the AuNR core. In contrast, the polymeric pyridine derivative, PVPy, was unable to do so, and no SERS signals were detected.

5.5 Potential applications of nanohybrids or synthesis of new MOF-based nanostructures

Hybrid nanostructures have also been synthesized, which have not been used for any application; however, it is expected that they may present potential applications in catalysis/photocatalysis and nanomedicine, for example, and even open the possibility of synthesizing new MOF structures around NPs for future applications (Fig. 13).

In the case of the AuNR@HKUST-1 (1) synthesized by LbL it is expected that this nanostructure presents potential applications in detection and catalysis.[36] Another example is the AuNR@MOF (2) nanohybrid; in summary, it could have potential applications in nanomedicine and photocatalysis.[39] Moreover, the universal applicability of this strategy opens access to diverse nanostructures surrounded by MOFs with the property of the core nanostructures complementing the functionality of the porphyrin MOF shell. The AuNR@MOF (4) nanohybrid will find numerous applications in optoelectronic devices, photocatalysis and nanomedicine.[45] Regarding the AuNR@HKUST-1 (2), it is highlighted that given the various studies on NP@MxOy core-shells showed in this article, this strategy may find its way to new structures, thus opening up fascinating perspectives for the development of porous MOF materials for future applications.[46] The use of the AuNR@ZIF-8 (1) nanohybrid in a particular application has not been reported; however, the capability to direct ZIF-8 growth by controlling the ligand assembly on the metallic NP surfaces opens new opportunities in the synthesis of MOF-based complex nanostructures for different applications.[43]

As we have seen, these nanohybrids have applications mainly in the biological field. The main advantages of using them in this area are their nanoscale size, biodegradability and biocompatibility. They enable controlled release of drugs, both *in vivo* and *in vitro* in the case of cancer treatments, and the release can be localized. Yet, these nanohybrids could produce ROS, linked to genetic instability and cancer.[89,90] Even though nanohybrids have demonstrated good molecular adsorption capacity that allows for high drug release capacity, the MOF pore size and molecule volume will be key factors in avoiding the limiting factors.

6. Conclusions and perspectives

Regarding the synthesis processes, it is indisputable that the selection of the solvents plays an important role in the AuNR synthesis, SAM process and MOF growth since they can generate or avoid agglomeration. Based on the studies currently carried out, the solvents mostly used in the formation of the SAM between the AuNR and the surface ligand are water, EtOH and MeOH. For the growth of the MOF, EtOH, DMF, water and MeOH are used in almost all cases.

The surface ligands selected to functionalize Au are the ones connected through Au–S covalent bonds, since they provide great stability. Furthermore, the ligands used in these studies can present important size differences, as is the case of MUA and PEG, for example, but they are still feasible to obtain the desired structure while protecting Au. However, the exposed end of the ligands, not linked to Au, have in general a COOH group that induces the MOF growth.

In addition, both the metallic centers and the carboxylic acid-based linkers (di, tri or tetratopic) used for the formation of MOFs are diverse, so they can be changed to obtain different types of MOF shells. This reveals the potential in the various types of applications that can be given to these coordination polymers around AuNRs.

It has also been shown that the methodologies to be used to generate the MOF shell, which surrounds the AuNRs, influence the shape that the MOF acquires around it, since different shapes can be obtained even using the same MOF components.

Undoubtedly, the AuNR@MOF nanohybrid structures analyzed in this study present quite defined morphologies and are also diverse. Most of the morphologies of MOFs around the AuNRs that were synthesized are rod-shaped and one is star-shaped. Other MOF morphologies obtained were cube, hexagonal and petal shapes, which presented greater thicknesses around the AuNR. In addition, in the vast majority of nanohybrids a single AuNR was obtained within the MOF crystalline structures.

In summary, different synthesis methodologies for AuNR@-MOF nanohybrids have been established since 2018. These nanohybrids have shown potential for use in several biological studies due to the complementary properties of AuNRs and MOFs. These nanoporous coordination polymers endow the nanohybrid material with stability in different environments and the nanosystems with multifunctional properties for drug uptake/release and analyte detection by SERS.

In addition, potential applications in catalysis, photocatalysis, or optoelectronics, for example, have yet to be explored. Based on the properties of MOFs, these nanohybrids could also be used as fluorescent sensors for the detection of contaminating metal ions in solvents. Less explored are the applications of nanohybrids of AuNRs and MOFs for fluorescence studies, where the SEF effect can be exerted by the plasmon.

A wide variety of surface ligands of different sizes with different metal centers and linkers that currently exist to generate MOFs open up the possibility of synthesizing a variety of new AuNR@MOF nanohybrids and targeting them towards a broad range of unexplored applications, such as those already mentioned. Therefore, we believe that future research directions and trends will be based on this type of nanohybrids with multifunctional capabilities for applications in different fields. However, it is necessary to evaluate the safety of these nanomaterials for the biological applications.

Author contributions

Aldo A. Campos joined to add bibliography and to request the authors of the articles included in this review for the inclusion of images. Marcelo J. Kogan and Monica Soler joined in the revision of introduction, discussions and conclusions, and Catherine E. Araneda prepared the manuscript, figures and tables. All authors reviewed the manuscript. All authors have given approval to the final version of the manuscript.

Conflicts of interest

There are no conflicts to declare.

Data availability

This feature article does not report original research data.

Acknowledgements

The authors are grateful to the ANID National Doctoral Scholarship (21220298), the Project Anillo (ACT210059), the Project FONDECYT (1251140), the Projects FONDAP (15130011 and 1523A0008) and the ENL17/25 Enlace Project, University of Chile, for financial project.

Notes and references

1 Y. A. Attia, T. A. Altalhi and A. A. Gobouri, *Adv. Nanopart.*, 2015, **04**, 85–97.
2 O. Donoso-González, L. Lodeiro, Á. E. Aliaga, M. A. Laguna-Bercero, S. Bollo, M. J. Kogan, N. Yutronic and R. Sierpe, *Pharmaceutics*, 2021, **13**, 261.
3 P. Jara-Guajardo, P. Cabrera, F. Celis, M. Soler, I. Berlanga, N. Parra-Muñoz, G. Acosta, F. Albericio, F. Guzman, M. Campos, A. Alvarez, F. Morales-Zavala and M. J. Kogan, *Nanomaterials*, 2021, **13**, 690.
4 N. R. Jana, L. Gearheart and C. J. Murphy, *J. Phys. Chem. B*, 2001, **105**, 4065–4067.
5 F. Morales-Zavala, H. Arriagada, N. Hassan, C. Velasco, A. Riveros, A. R. Álvarez, A. N. Minniti, X. Rojas-Silva, L. L. Muñoz, R. Vasquez, K. Rodriguez, M. Sanchez-Navarro, E. Giralt, E. Araya, R. Aldunate and M. J. Kogan, *Nanomedicine*, 2017, **13**, 2341–2350.
6 M. P. Oyarzún, A. Tapia-Arellano, P. Cabrera, P. Jara-Guajardo and M. J. Kogan, *Sensors*, 2021, **21**, 2067.
7 M. P. Oyarzún, P. Cabrera, N. Parra-Muñoz, V. López, A. Riveros, F. Celis, R. Gimeno-Muñoz, A. González-Campo, N. Aliaga-Alcalde, M. Soler and M. J. Kogan, *Colloids Surf., B*, 2025, **252**, 114660.
8 M. Suzuki, Y. Niidome and S. Yamada, *Thin Solid Films*, 2006, **496**, 740–747.
9 B. Nikoobakht and M. A. El-Sayed, *Chem. Mater.*, 2003, **15**, 1957–1962.
10 P.-J. Huang, C.-K. Lee, L.-H. Lee, H.-F. Huang, Y.-H. Huang, J.-C. Lan and C.-H. Lee, *Skin Res Technol.*, 2023, **29**, e13334.
11 S. Chang, H. Ko, S. Singamaneni, R. Gunawidjaja and V. V. Tsukruk, *Anal. Chem.*, 2009, **81**, 5740–5748.
12 N. Albarghouthi, P. MacMillan and C. L. Brosseau, *Analyst*, 2021, **146**, 2037–2047.
13 K. Sugikawa, Y. Furukawa and K. Sada, *Chem. Mat.*, 2011, **23**, 3132–3134.
14 K. Sugikawa, S. Nagata, Y. Furukawa, K. Kokado and K. Sada, *Chem. Mater.*, 2013, **25**, 2565–2570.
15 A. Abbasi, T. Moradpour and K. Van Hecke, *Inorg. Chim. Acta*, 2015, **430**, 261–267.
16 J. Guo, J. F. Ma, B. Liu, W. Q. Kan and J. Yang, *Cryst. Growth Des.*, 2011, **11**, 3609–3621.
17 L. Liu, Y. Zhou, S. Liu and M. Xu, *Chem. Electro. Chem.*, 2018, **5**, 6–19.
18 P. Horcajada, R. Gref, T. Baati, P. K. Allan, G. Maurin, P. Couvreur, G. Férey, R. E. Morris and C. Serre, *Chem. Rev.*, 2012, **112**, 1232–1268.
19 K. Sumida, D. L. Rogow, J. A. Mason, T. M. McDonald, E. D. Bloch, Z. R. Herm, T. H. Bae and J. R. Long, *Chem. Rev.*, 2012, **112**, 724–781.
20 R. Fu, W. Li, G. He, D. He and H. Chen, *Mol. Catal.*, 2025, **573**, 114811.

21 M. Kim, M. Pander and H. R. Moon, *ACS Appl. Electron. Mater.*, 2024, **6**, 3024–3038.
22 Y. Cai, T. Dong, Z. Bian, H. Liu, X. Liu and A. Liu, *Coord. Chem. Rev.*, 2025, **529**, 216470.
23 S. Zhao, Y. Zhang, S. Ding, J. Fan, Z. Luo, K. Liu, Q. Shi, W. Liu and G. Zang, *J. Electroanal. Chem.*, 2019, **834**, 33–42.
24 L. He, Y. Liu, J. Liu, Y. Xiong, J. Zheng, Y. Liu and Z. Tang, *Angew. Chem., Int. Ed.*, 2013, **52**, 3741–3745.
25 C. Wang, N. Zhang, Y. Li, L. Yang, D. Wei, T. Yan, H. Ju, B. Du and Q. Wei, *Sens. Actuators B: Chem.*, 2019, **291**, 319–328.
26 Y. Zhou, C. Li, X. Li, X. Zhu, B. Ye and M. Xu, *Anal. Methods*, 2018, **10**, 4430–4437.
27 G. Zhao, Y. Wang, X. Li, Q. Yue, X. Dong, B. Du, W. Cao and Q. Wei, *Anal. Chem.*, 2019, **91**, 1989–1996.
28 A. Dhakshinamoorthy and H. Garcia, *Chem. Soc. Rev.*, 2012, **41**, 5262–5284.
29 M. Chalermnon, S. R. Thomas, J. M. Chin and M. R. Reithofer, *Inorg. Chem. Front.*, 2025, **12**, 6435–6459.
30 M. Meilikhov, K. Yusenko, D. Esken, S. Turner, G. Van Tendeloo and R. A. Fischer, *Eur. J. Inorg. Chem.*, 2010, **2010**, 3701–3714.
31 H. Zhou, A. Zhu, C. Wang, X. Guo, Y. Ying, Y. Wu, X. Liu, F. Wang, Y. Wen and H. Yang, *Spectrochim. Acta A Mol. Biomol. Spectrosc.*, 2024, **304**, 123280.
32 X. Cao, S. Hong, Z. Jiang, Y. She, S. Wang, C. Zhang, H. Li, F. Jin, M. Jin and J. Wang, *Analyst*, 2017, **142**, 2640–2647.
33 Y. Liu and Z. Tang, *Adv. Mater.*, 2013, **25**, 5819–5825.
34 H. R. Moon, D. W. Lim and M. P. Suh, *Chem. Soc. Rev.*, 2013, **42**, 1807–1824.
35 J. G. Turner and C. J. Murphy, *Langmuir*, 2021, **37**, 9910–9919.
36 J. G. Hinman, J. G. Turner, D. M. Hofmann and C. J. Murphy, *Chem. Mater.*, 2018, **30**, 7255–7261.
37 H. Guo, S. Yi, K. Feng, Y. Xia, X. Qu, F. Wan, L. Chen and C. Zhang, *Chem. Eng. J.*, 2021, **403**, 126432.
38 K. Khaletskaya, J. Reboul, M. Meilikhov, M. Nakahama, S. Diring, M. Tsujimoto, S. Isoda, F. Kim, K. I. Kamei, R. A. Fischer, S. Kitagawa and S. Furukawa, *J. Am. Chem. Soc.*, 2013, **135**, 10998–11005.
39 J. Y. Zeng, X. S. Wang, M. K. Zhang, Z. H. Li, D. Gong, P. Pan, L. Huang, S. X. Cheng, H. Cheng and X. Z. Zhang, *ACS Appl. Mater. Interfaces*, 2017, **9**, 43143–43153.
40 J. Y. Zeng, M. K. Zhang, M. Y. Peng, D. Gong and X. Z. Zhang, *Adv. Funct., Mater.*, 2018, **28**, 1705451.
41 J. W. M. Osterrieth, D. Wright, H. Noh, C. W. Kung, D. Vulpe, A. Li, J. E. Park, R. P. Van Duyne, P. Z. Moghadam, J. J. Baumberg, O. K. Farha and D. Fairen-Jimenez, *J. Am. Chem. Soc.*, 2019, **141**, 3893–3900.
42 W. Shang, C. Zeng, Y. Du, H. Hui, X. Liang, C. Chi, K. Wang, Z. Wang and J. Tian, *Adv. Mater.*, 2017, **29**, 1604381.
43 J. He, R. C. C. Yap, S. Yee Wong, Y. Zhang, Y. Hu, C. Chen, X. Zhang, J. Wang and X. Li, *Cryst. Eng. Comm.*, 2016, **18**, 5262–5266.
44 Y. Li, J. Jin, D. Wang, J. Lv, K. Hou, Y. Liu, C. Chen and Z. Tang, *Nano Res.*, 2018, **11**, 3294–3305.
45 Z. Zhou, M. Li, J. Zhao, Z. Di, C. Di, B. Liu, C. Zhang, C. H. Yan and L. Li, *Chem. Commun.*, 2018, **54**, 8182–8185.
46 Y. Liu, W. Zhang, S. Li, C. Cui, J. Wu, H. Chen and F. Huo, *Chem. Mater.*, 2014, **26**, 1119–1125.
47 G. Li, S. Zhao, Y. Zhang and Z. Tang, *Adv. Mater.*, 2018, **30**, 1800702.
48 L. Scarabelli, A. Sánchez-Iglesias, J. Pérez-Juste and L. M. Liz-Marzán, *J. Phys. Chem. Lett.*, 2015, **6**, 4270–4279.
49 J. Pérez-Juste, I. Pastoriza-Santos, L. M. Liz-Marzán and P. Mulvaney, *Coord. Chem. Rev.*, 2005, **249**, 1870–1901.
50 C. J. Murphy, T. K. Sau, A. M. Gole, C. J. Orendorff, J. Gao, L. Gou, S. E. Hunyadi and T. Li, *J. Phys. Chem. B*, 2005, **109**, 13857–13870.
51 N. Li, P. Zhao and D. Astruc, *Angew. Chem., Int. Ed.*, 2014, **53**, 1756–1789.
52 N. D. Burrows, W. Lin, J. G. Hinman, J. M. Dennison, A. M. Vartanian, N. S. Abadeer, E. M. Grzincic, L. M. Jacob, J. Li and C. J. Murphy, *Langmuir*, 2016, **32**, 9905–9921.
53 Y. Xia, J. A. Rogers, K. E. Paul, G. M. Whitesides, B. R. Nikhil Jana, L. Gearheart, C. J. Murphy, N. R. Jana, L. Gearheart and C. J. Murphy, *Adv. Mater.*, 2001, **99**, 1389–1393.
54 M. Sidorova and A. Popov, *Chem. Proc.*, 2023, **14**, 11–15.
55 A. M. Alkilany, A. I. B. Yaseen, J. Park, J. R. Eller and C. J. Murphy, *RSC Adv.*, 2014, **4**, 52676–52679.
56 S. Nath, S. K. Ghosh, S. Kundu, S. Praharaj, S. Panigrahi and T. Pal, *J. Nanoparticle Res.*, 2006, **8**, 111–116.
57 A. M. Smith, L. E. Marbella, K. A. Johnston, M. J. Hartmann, S. E. Crawford, L. M. Kozycz, D. S. Seferos and J. E. Millstone, *Anal. Chem.*, 2015, **87**, 2771–2778.
58 J. Jiang, C. V. Conroy, M. M. Kvetny, G. J. Lake, J. W. Padelford, T. Ahuja and G. Wang, *J. Phys. Chem. C*, 2014, **118**, 20680–20687.
59 J. He, Y. Wang, Y. Feng, X. Qi, Z. Zeng, Q. Liu, W. S. Teo, C. L. Gan, H. Zhang and H. Chen, *ACS Nano*, 2013, **7**, 2733–2740.
60 J. He, Y. Wang, Z. Fan, Z. Lam, H. Zhang, B. Liu and H. Chen, *Nanoscale*, 2015, **7**, 8115–8121.
61 J. He, W. Ji, L. Yao, Y. Wang, B. Khezri, R. D. Webster and H. Chen, *Adv. Mater.*, 2014, **26**, 4151–4155.
62 J. C. Love, L. A. Estroff, J. K. Kriebel, R. G. Nuzzo and G. M. Whitesides, *Chem. Rev.*, 2005, **105**, 1103–1169.
63 S. Haesuwannakij, T. Kimura, Y. Furutani, K. Okumura, K. Kokubo, T. Sakata, H. Yasuda, Y. Yakiyama and H. Sakurai, *Sci. Rep.*, 2017, **7**, 9579–9587.
64 A. Alijagic, A. Bonura, F. Barbero, V. F. Puntes, F. Gervasi and A. Pinsino, *Nanomaterials*, 2021, **11**, 2646–2663.
65 Q. Hua, D. Shang, W. Zhang, K. Chen, S. Chang, Y. Ma, Z. Jiang, J. Yang and W. Huang, *Langmuir*, 2011, **27**, 665–671.
66 H. Ridaoui, A. Jada, L. Vidal and J. B. Donnet, *Colloids Surf., A*, 2006, **278**, 149–159.
67 S. Bahrani, S. A. Hashemi, S. M. Mousavi and R. Azhdari, *Drug Metab. Rev.*, 2019, **51**, 356–377.
68 N. Singh, S. Qutub and N. M. Khashab, *J. Mater. Chem. B*, 2021, **9**, 5925–5934.
69 Y. Hu, S. Bai, X. Wu, S. Tan and Y. He, *Ceram. Int.*, 2021, **47**, 31031–31041.
70 Q. Shi, Y. Zhao, M. Liu, F. Shi, L. Chen, X. Xu, J. Gao, H. Zhao, F. Lu, Y. Qin, Z. Zhang and M. Lian, *Small*, 2024, **20**, 2309366.

71 R. Ettlinger, U. Lächelt, R. Gref, P. Horcajada, T. Lammers, C. Serre, P. Couvreur, R. E. Morris and S. Wuttke, *Chem. Soc. Rev.*, 2022, **51**, 464–484.
72 D. Jiang, C. Huang, J. Zhu, P. Wang, Z. Liu and D. Fang, *Coord. Chem. Rev.*, 2021, **444**, 214064.
73 C. Atzori, G. C. Shearer, L. Maschio, B. Civalleri, F. Bonino, C. Lamberti, S. Svelle, K. P. Lillerud and S. Bordiga, *J. Phys. Chem. C*, 2017, **121**, 9312–9324.
74 W. Cai, J. Yu and M. Jaroniec, *J. Mater. Chem.*, 2011, **21**, 9066–9072.
75 J. Reboul, S. Furukawa, N. Horike, M. Tsotsalas, K. Hirai, H. Uehara, M. Kondo, N. Louvain, O. Sakata and S. Kitagawa, *Nat. Mater.*, 2012, **11**, 717–723.
76 H. Noh, C. W. Kung, T. Islamoglu, A. W. Peters, Y. Liao, P. Li, S. J. Garibay, X. Zhang, M. R. Destefano, J. T. Hupp and O. K. Farha, *Chem. Mater.*, 2018, **30**, 2193–2197.
77 G. Lu, S. Li, Z. Guo, O. K. Farha, B. G. Hauser, X. Qi, Y. Wang, X. Wang, S. Han, X. Liu, J. S. Duchene, H. Zhang, Q. Zhang, X. Chen, J. Ma, S. C. J. Loo, W. D. Wei, Y. Yang, J. T. Hupp and F. Huo, *Nat. Chem.*, 2012, **4**, 310–316.
78 X. Huang, B. Zheng, Z. Liu, C. Tan, J. Liu, B. Chen, H. Li, J. Chen, X. Zhang, Z. Fan, W. Zhang, Z. Guo, F. Huo, Y. Yang, L. H. Xie, W. Huang and H. Zhang, *ACS Nano*, 2014, **8**, 8695–8701.
79 H. X. Zhong, J. Wang, Y. W. Zhang, W. L. Xu, W. Xing, D. Xu, Y. F. Zhang and X. B. Zhang, *Angew. Chem., Int. Ed.*, 2014, **53**, 14235–14239.
80 L. Liu, Q. Yuan, J. Shi, X. Li, D. Jung, L. Wang, K. Yamauchi, N. Nakatsuji, K. ichiro Kamei and Y. Chen, *Biotechnol. Lett.*, 2012, **34**, 1951–1957.
81 A. Albanese, P. S. Tang and W. C. W. Chan, *Annu. Rev. Biomed. Eng.*, 2012, **14**, 1–16.
82 C. J. Murphy, H. H. Chang, P. Falagan-Lotsch, M. T. Gole, D. M. Hofmann, K. N. L. Hoang, S. M. McClain, S. M. Meyer, J. G. Turner, M. Unnikrishnan, M. Wu, X. Zhang and Y. Zhang, *Acc. Chem. Res.*, 2019, **52**, 2124–2135.
83 A. M. Alkilany, S. E. Lohse and C. J. Murphy, *Acc. Chem. Res.*, 2013, **46**, 650–661.
84 D. Baimanov, R. Cai and C. Chen, *Bioconjugate Chem.*, 2019, **30**, 1923–1937.
85 C. J. Murphy, A. M. Vartanian, F. M. Geiger, R. J. Hamers, J. Pedersen, Q. Cui, C. L. Haynes, E. E. Carlson, R. Hernandez, R. D. Klaper, G. Orr and Z. Rosenzweig, *ACS. Cent. Sci.*, 2015, **1**, 117–123.
86 T. W. Odom and G. C. Schatz, *Chem. Rev.*, 2011, **111**, 3667–3668.
87 K. M. Mayer and J. H. Hafner, *Chem. Rev.*, 2011, **111**, 3828–3857.
88 S. Schlücker, *Angew. Chem.*, 2014, **53**, 4756–4795.
89 S. Ju, M. K. Singh, S. Han, J. Ranbhise, J. Ha, W. Choe, K.-S. Yoon, S. G. Yeo, S. S. Kim and I. Kang, *Int. J. Mol. Sci.*, 2024, **25**, 12387.
90 R. Tiwari, Y. Mondal, K. Bharadwaj, M. Mahajan, S. Mondal and A. Sarkar, *Drug Dev. Res.*, 2025, **86**, e70107.